# HYBRID REGULARIZATION FOR MRI RECONSTRUCTION WITH STATIC FIELD INHOMOGENEITY CORRECTION

*Ryan Compton, Stanley Osher*

University of California, Los Angeles
Department of Mathematics
Los Angeles, CA 90095-1555

*Louis Bouchard*

University of California, Los Angeles
Department of Chemistry
Los Angeles, CA 90095-1555

## ABSTRACT

Rapid acquisition of magnetic resonance (MR) images via reconstruction from undersampled $k$-space data has the potential to greatly decrease MRI scan time on existing medical hardware. To this end iterative image reconstrction based on the technique of compressed sensing has become the method choice for many researchers [1]. However, while conventional compressed sensing relies on random measurements from a discrete Fourier transform, actual MR scans often suffer from off-resonance effects and thus generate data by way of a non-Fourier operator, complicating image reconstruction methods and introducing additional computational bottlenecks [2]. In this work we introduce a combined TV-framelet regularization to the undersampled MR reconstruction problem in inhomogeneous fields. We show that the inclusion of a framelet regularization term decreases computation time and improves image quality over the traditional total variation (TV)-based approach.

## 1. INTRODUCTION

While the problem of image reconstruction in magnetic resonance imaging (MRI) has a long history, the techniques employed usually assume the static magnetic field is homogeneous and the applied magnetic-field gradients are unidirectional with constant magnitude [3]. In recent years, the prospects of generating MRI images using portable sensors have been explored [4][5]. Although some efforts have focused on generating remote homogeneous fields [6] [7], most portable sensors are single-sided and characterized by inhomogeneous fields [8] [9]. The inhomogeneous field can be used to select a slice for imaging [4]. In other instances, so-called "shimming" radio-frequency (RF) pulses have been used to prepare the spins and impart a phase that compensates for the effects of an inhomogeneous field [10][11][12]. In the limit of low magnetic fields, the magnetic-field gradients are no longer unidirectional according to Maxwell's equations in the absence of a rotating-wave approximation. MRI is still feasible with the use of coherent averaging techniques [13][14], oscillating fields [15] or spatial shimming [16]. Each of these techniques have limitations. For coherent averaging and RF shimming techniques, the stroboscopic sequences required are not practical for *in vivo* use because of RF heating and the short $T_2$ relaxation times in tissues. In this article, we treat the problem of image reconstruction in high-field MRI, in the presence of inhomogeneous static and gradient magnetic fields. The direct reconstruction (as opposed to the use of compensating techniques) may be the preferred approach in clinical applications, where rapid imaging is required.

The most general MRI reconstruction problem assumes no rotating-wave approximation. Spins precess about a field $\vec{B}(\mathbf{r},t)$ which may include time-dependent gradients. Its direction and magnitude may be a function of space. Because of the time-dependence of the local field, the rotations are non-commutative and a time-ordered product must be used to describe its effect. For spin $I = 1/2$, the rotations are described by the spin operators $I_i = \sigma_i/2$, $i = x, y, z$, where $\sigma_i$ are the Pauli matrices. The rotation operator is written in terms of Dyson time-ordering $\vec{T}$:

$$U(\mathbf{r},t) = \vec{T}e^{i\gamma\int_0^t [I_x B_x(\mathbf{r},t)+I_y B_y(\mathbf{r},t)+I_z B_z(\mathbf{r},t)]dt}$$

The initial state of the nuclear magnetization density can be expressed as $\rho(\mathbf{r}) = I_x\rho_x(\mathbf{r}) + I_y\rho_y(\mathbf{r}) + I_z\rho_z(\mathbf{r})$. It is evolved in time according to the unitary transformation $\rho(\mathbf{r},T) = U^\dagger(\mathbf{r},T)\rho(\mathbf{r})U(\mathbf{r},T)$. Detection is done along a given axis defined by a field $\vec{B}_1(\mathbf{r})$. Neglecting relaxation effects, the NMR signal is therefore proportional to the volume integral of the Hilbert space trace (Tr):

$$\begin{aligned} s(t) = \int_V \mathrm{Tr}[\{&B_{1x}(\mathbf{r})I_x + B_{1y}(\mathbf{r})I_y \\ &+ B_{1z}(\mathbf{r})I_z\}U^\dagger(\mathbf{r},t)\rho(\mathbf{r})U(\mathbf{r},t)]d^3\mathbf{r}. \end{aligned} \tag{1}$$

The image reconstruction problem consists of solving for the magnetization distribution $\rho(\mathbf{r})$ by measuring $s(t)$ at different times $t$ while time-modulating the gradients.

If a strong static magnetic field is applied, only the components of the magnetic field gradients parallel to the static magnetic field are preserved. The perpendicular components of the gradient fields rapidly average to zero. This rotating-wave approximation leads to a local magnetic field whose direction remains fixed. Only its magnitude can change with time. Therefore, time-ordered rotations are no longer needed. The signal equation reduces to a simpler expression:

$$s(t) = \int_V \rho(\mathbf{r}) e^{-z(\mathbf{r})t} e^{-2\pi i \mathbf{k}(t)\cdot\mathbf{r}} d\mathbf{r} \tag{2}$$

where $s(t_i)$ is the recorded signal, $z(\mathbf{r})$ describes the off-resonance effects (imaginary part). Relaxation effects can be included in $z(\mathbf{r})$ (real part). The magnetization density, $\rho(\mathbf{r})$, is a scalar-valued field. The goal of MRI reconstruction is to solve for the proton density map, $\rho(\mathbf{r})$, in the signal equation. The $k$-space coordinates, $\mathbf{k}(t)$, which are defined by the applied gradients, are known only on a nonuniform and possibly undersampled grid [17]. The gradients are assumed to be uniform. For a 2D slice, $V$ is a subset of $\mathbb{R}^2$.

A $n$-point discretization of the physical space integral at $m$ different values of $t$ leads to the $m \times n$ linear system

$$s = A\rho \tag{3}$$

with system matrix

$$A_{ij} = e^{-z(\mathbf{r}_j)t_i} e^{-2\pi i \mathbf{k}(t_i)\cdot\mathbf{r}_j}. \tag{4}$$

The goal of MRI reconstruction is to efficiently invert the linear system (3) in a way that produces high quality images. With conventional MRI methods, the background field is assumed perfectly homogeneous and the phase accrual due to off resonant frequency, $e^{-z(\mathbf{r}_j)t_i}$, is then ignored. Recording all points in $k$-space on a uniform grid allows estimation of $\rho$ by inverting a single Fourier transform.

While simple computationally, failing to accommodate for off-resonance effects often leads to blurring and image distortion in many types of MR scans. Caused by static field inhomogeneities, these off-resonance effects manifest themselves in scans with long readout times as well as scans near air/tissue interfaces where magnetic susceptibility variations are exacerbated [18]. This is of specific importance for surgical planning near the nasal sinuses, ears, and cerebral cortex [19].

Conversely, directing forming $A$ is infeasible for practical image sizes. As a result, methods of operator compression based on combinations of Fourier operators have been developed to efficient apply $A$ allowing one to use iterative methods to solve for $\rho$ [20].

Provided enough $k$-space data has been recorded these iterative methods are very reliable [21]. However, in the absence of off-resonance effects, the field of compressed sensing has shown that exact image reconstruction is possible from extremely sparse $k$-space [22].

In this work we propose solutions to rectify these two issues, demonstrating a method for image recovery with a generalized operator when $k$-space is undersampled. Furthermore, we introduce a regularization term based on framelets which reduces the computational costs associated with a standard compressed sensing based reconstruction.

## 2. METHOD

### 2.1. Low rank inhomogeneity correction

Separable low rank approximations to the off-resonance matrix, $E_{ij} = e^{-z(\mathbf{r}_j)t_i}$, allow us to rapidly apply $A$ with little storage overhead. For a given rank, $L$, we form $B \in \mathbb{R}^{m\times L}$ and $C \in \mathbb{R}^{L\times n}$ minimizing $\|E - BC\|_2$ using the methods of [21]. This yields the general system matrix

$$A = \sum_{l=1}^{L} B_l \mathcal{G} C_l \tag{5}$$

where $B_l$ and $C_l$ are diagonal matrices ($B_l = diag(B_{il})$, $C_l = diag(C_{lj})$), and $\mathcal{G}$ is a nonuniform discrete Fourier transform (NUFFT) of type 2.

While fast to apply, the modified system matrix obeys uncertainty properties differing from the pure Fourier case.

Recall the concept of a *restricted isometry constant*, $\delta_s^A$, of a matrix $A$ for an integer $s$ as the smallest number such that

$$(1-\delta_s^A)\|x\|_{l2}^2 \le \|Ax\|_{l2}^2 \le (1+\delta_s^A)\|x\|_{l2}^2 \tag{6}$$

where $s$ is the number of nonzero entries in $x$. When such a constant exists $A$ is said to satisfy the *restricted isometry property*. This property guarantees exact image reconstruction from vastly undersampled $k$-space with overwhelmingly high probability. In the case of an undersampled Fourier matrix, much work has been devoted to showing that $\delta_s^{\mathcal{G}}$ is small [23].

In our corrected system matrix we can infer that each term in the sum (5) has less than ideal isometric properties by examining

$$\begin{aligned} \|B_l\mathcal{G}C_l x\|_2 &\le \|B_l\|\|\mathcal{G}C_l x\|_2 &(7)\\ &\le \max_i(b_{il})(1+\delta_s^{\mathcal{G}})\max_j(c_{lj})\|x\|_2 &(8)\end{aligned}$$

By combining (8) with the analogous lower bound a crude estimate for the restricted isometry constant for an $L = 1$ correction to our inhomogeneity can be found

$$\begin{aligned}\delta_s^{B_l\mathcal{G}C_l} \le \min\Big(&1 - \min_i(b_{il})\min_j(c_{lj}) \\ &+ \min_i(b_{il})\min_j(c_{lj})\delta_s^{\mathcal{G}},\ 1 - \max_i(b_{il})\max_j(c_{lj}) \\ &+ \max_i(b_{il})\max_j(c_{lj})\delta_s^{\mathcal{G}}\Big).\end{aligned} \tag{9}$$

Larger values for $L$ increase the corresponding isometry constants and as a result more samples are required for accurate image recovery than in the pure Fourier case.

### 2.2. Sparse recovery via $l1$ minimization

We propose a reduction in scan time by appealing to the theory of compressed sensing, downsampling our Fourier matrix uniformly at random and accounting for the missing data with sparsity promoting regularization. The canonical image reconstruction problem is

$$\underset{\rho}{argmin}\, J(\rho) \text{ subject to } A\rho = s \tag{10}$$

where $J$ represents some form of $l1$ regularization.

While MR images are not sparse in the image domain, they are sparse in an appropriately chosen transform domain [1]. Representation of images in bases of wavelets, and by extension, framelets yield sparse collections of coefficients. Similarly, reconstruction methods based on the total variation norm well as its nonlocal counterpart have been shown to accurately reproduce detailed images from sparse frequency data [24].

In this work we advocate a composite of total variation and framelet regularization,

$$J(\rho) = |\nabla\rho| + |F\rho| \tag{11}$$

where the first term is a total variation norm and $F$ is the discrete framelet decomposition [25]. The total variation term enhances edges in our reconstructed image while the inclusion of the framelet term allows us to reconstruct smooth images.

It has been found previously that hybrid regularization based on wavelets often improves image quality [26]. Our framelet based regularization extends this work to redundant orthogonal bases where natural images can be represented more accurately.

In fact, not only does our hybrid regularization improve image quality, it markedly decreases computational cost when compared with a solitary total variation regularizer as the subproblems we solve in our minimization become better conditioned.

### 2.3. Split Bregman iterations for image recovery

Our image is the solution to the constrained optimization (10) which we solve with the Split Bregman method of [26]. We begin by converting the constrained optimization into a sequence of unconstrained problems via Bregman iteration

$$\begin{cases} \rho^{k+1} &= \min_\rho |\nabla\rho| + |F\rho| + \frac{\mu}{2}\|A\rho - s^k\|^2 \\ s^{k+1} &= s^k + s - A\rho^{k+1} \end{cases} \tag{12}$$

where the parameter $\mu$ affects the convergence rate and is chosen by the user. Alternately updating $\rho^k$ and $s^k$ produces a sequence $\rho^k \to \rho$, the solution to the constrained problem.

Updating $s^k$ is straightforward. Minimization of the unconstrained step in (12) is done by introducing auxiliary variables, $d_x = \nabla_x\rho$, $d_y = \nabla_y\rho$, and $w = F\rho$, allowing us to rewrite our $\rho^k$ update in the equivalent split form

$$\rho^{k+1} = \min_\rho |\nabla d| + |w| + \tfrac{\mu}{2}\|A\rho - s^k\|^2 \tag{13}$$

$$\text{subject to} \begin{cases} (d_x, d_y) = (\nabla_x\rho, \nabla_y\rho) \\ w = F\rho \end{cases} \tag{14}$$

This constrained optimization is then converted to a sequence of unconstrained problems via a second Bregman iteration leading us to the following algorithm:

**Algorithm 1**: Split Bregman iteration for constrained optimization

**Initialize**: $\rho^0 = A^t s$, and
$d_x^0 = d_y^0 = w^0 = b_x^0 = b_y^0 = b_w^0 = 0$
**while** $\|A\rho^k - s\|_2^2 > tol$ **do**
  **for** $i = 1$ *to* $n_{inner}$ **do**
    $\rho^{k+1} = \min_\rho \frac{\mu}{2}\|A\rho - s^k\|^2 + \frac{\lambda}{2}\|d_x^k - \nabla_x\rho - b_x^k\|^2 + \frac{\lambda}{2}\|d_x^k - \nabla_x\rho - b_x^k\|^2 + \frac{\gamma}{2}\|w^k - F\rho - b_w^k\|^2$
    $d_x^{k+1} = shrink(\nabla_x\rho^{k+1} + b_x^k, 1/\lambda)$
    $d_y^{k+1} = shrink(\nabla_y\rho^{k+1} + b_y^k, 1/\lambda)$
    $w^{k+1} = shrink(F\rho^{k+1} + b_w^k, 1/\gamma)$
    $b_x^{k+1} = b_x^k + (\nabla_x\rho^{k+1} - d_x^{k+1})$
    $b_y^{k+1} = b_y^k + (\nabla_y\rho^{k+1} - d_y^{k+1})$
    $b_w^{k+1} = b_w^k + (F\rho^{k+1} - w^{k+1})$
  **end**
  $s^{k+1} = s^k + s - A\rho^{k+1}$
**end**

Here, the function $shrink$ comes from the wavelet literature and is defined as

$$shrink(x, a) = \frac{x}{|x|}\max(|x| - a, 0). \tag{15}$$

The constants $\lambda$ and $\gamma$ are chosen by the user and affect the convergence rate.

Computationally, the $\rho^{k+1}$ update is the most expensive part of our algorithm by a wide margin. The speed of our image reconstruction is thus largely determined by how fast we can solve this minimization. In the purely Fourier case an analytic solution exists leading to a notably fast algorithm [26]. We have no such formula for the generalized $A$ we work with and instead rely on iterations of the conjugate gradient method to update $\rho^{k+1}$.

By differentiating with respect to $\rho$ and setting the result to zero we find our $\rho^{k+1}$ update as the solution to

$$(\mu A^t A + \lambda\nabla_x^t\nabla_x + \lambda + \gamma F^t F)\rho^{k+1} = rhs^k \tag{16}$$

where

$$rhs^k = \mu A^t s^k + \lambda\nabla_x^t(d_x^k - b_x) + \lambda\nabla_y^t + \gamma F^t(w - b_w). \tag{17}$$

Making use of the identities $\nabla^t\nabla = -\triangle$ and $F^tF = I$, gives the system

$$(\mu A^t A - \lambda\triangle + \gamma I)\rho^{k+1} = rhs^k \tag{18}$$

which we solve with conjugate gradient iterations.

A major advantage of our hybrid regularizer is now apparent. Consider the system resulting from a regularization based only on total variation (ie $\gamma = 0$),

$$(\mu A^t A - \lambda\triangle)\rho^{k+1} = rhs^k. \tag{19}$$

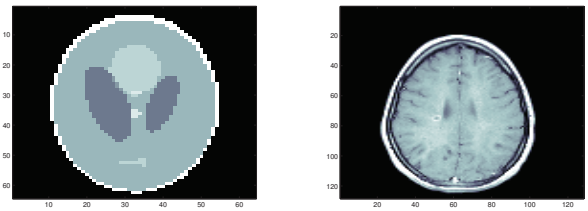
Denoting maximal and minimal eigenvalues of the matrix in (19) by $\lambda_{\max}$ and $\lambda_{\min}$ we can write the condition number of our hybrid regularized system as

$$\frac{\lambda_{\max} + \gamma}{\lambda_{\min} + \gamma} < \frac{\lambda_{\max}}{\lambda_{\min}} \tag{20}$$

notably speeding our updates.

## 3. NUMERICAL RESULTS

Our hybrid reconstruction method is compared against three alternate approaches: uncorrected nonuniform-FFT, field corrected total variation regularization, and field corrected framelet regularization.



64x64 phantom 128x128 brain image

**Fig. 1:** Exact images used for simulations.

The nonuniform Fourier transforms are computed with the min-max method of [27] using 6 points of interpolation. Piecewise linear B-spline framelets [25] are used in all simulations. The approximation is done with $L = 6$.

| Reduction factor | NUFFT | TV | Framelet | Hybrid |
|---|---|---|---|---|
| 1.5x | 1.0954e+04 | 0.3134 | 0.3134 | 0.3621 |
| 2.5x | 1.2032e+04 | 32.0884 | 14.3459 | 9.9995 |
| 3.5x | 1.2369e+04 | 35.0548 | 21.8537 | 18.3263 |
| 4.5x | 1.2536e+04 | 48.4947 | 44.9358 | 43.8486 |

**Table 1:** Brain image reconstruction error: $\|\rho_{exact} - \rho\|_2$

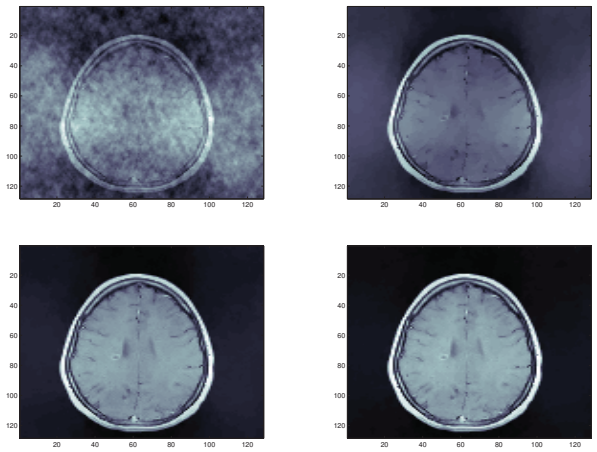


**Fig. 2:** Brain image reconstruction at 2.5x undersampling. Clockwise from top left: NUFFT, TV, TV-Framelet, and Framelet regularizations. All iterative methods were stopped after 3000 applications of $A$.

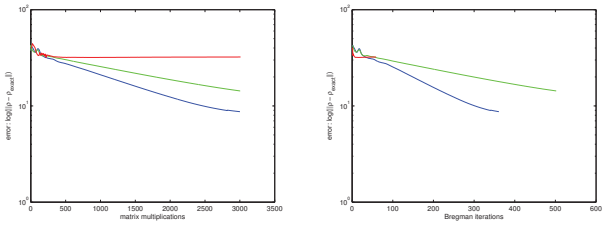


**Fig. 3:** Brain image reconstruction errors after 3000 applications of $A$ at 2.5x undersampling. Image domain error, $\log\|\rho - \rho_{exact}\|$. TV, framelet, and hybrid regularization in red, green, and blue, respectively. Splitting parameter $\mu = 1$, $\lambda = 0.5$, and $\gamma = 25$.

Plotting errors per iteration in Figs. 3 and 4 we see that total variation is the most efficient per Bregman update. However, as Table 1 shows, hybrid and framelet based methods outperform total variation significantly when taking into account the number of matrix multiplications.

## 4. CONCLUSION

We have presented an efficient and fast-converging algorithm for MRI image reconstruction in the presence of inhomogeneous fields. This requires knowledge of the $k$-space trajectory and field inhomogeneity profile. The latter could be obtained in real time using $B_0$ mapping techniques. The former is prescribed by the imaging pulse sequence. The technique

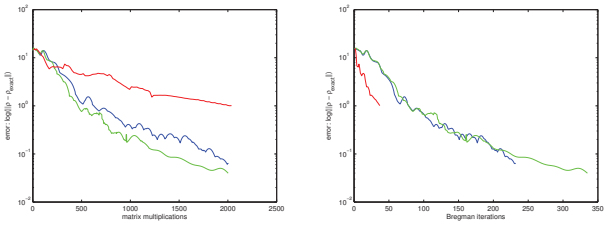



**Fig. 4:** Reconstruction errors on phantom after 2000 applications of $A$ at 3x undersampling.

should be applicable to the class of problems where the signal is a linear function of the spin density, $s = A\rho$, and the matrix $A$ can be decomposed into inhomogeneity and spatial encoding matrices. We note that the case of low-field MRI, the signal equation (1) is also of the form $s = A\rho$, where $A$ can be separated into encoding and inhomogeneity matrices. One difference is that computational overhead is increased due to the requirement for computing products of non-commutative rotation matrices. A more important difference is that the encoding matrix is no longer of type NUFFT. It is unclear at this stage if such non-NUFFT matrices would lead to convergence of our algorithm. Further investigations would be needed.

# References


[1] Michael Lustig, David Donoho, and John M Pauly, "Sparse MRI: The application of compressed sensing for rapid MR imaging.," *Magnetic resonance in medicine : official journal of the Society of Magnetic Resonance in Medicine / Society of Magnetic Resonance in Medicine*, vol. 58, no. 6, pp. 1182–95, Dec. 2007.

[2] J.a. Fessler, V.T. Olafsson, H.R. Shi, and D.C. Noll, "Toeplitz-based iterative image reconstruction for MRI with correction for magnetic field inhomogeneity," *IEEE Transactions on Signal Processing*, vol. 53, no. 9, pp. 3393–3402, Sept. 2005.

[3] P. Mansfield, *NMR Imaging in Biomedicine (Advances in magnetic resonance)*, Academic Press, 1982.

[4] Pablo J. Prado, "Single sided imaging sensor," *Magnetic Resonance Imaging*, vol. 21, no. 3-4, pp. 397–400, Apr. 2003.

[5] J Perlo, "3D imaging with a single-sided sensor: an open tomograph," *Journal of Magnetic Resonance*, vol. 166, no. 2, pp. 228–235, Feb. 2004.

[6] JL Paulsen, John Franck, Vasiliki Demas, and Louis-S. Bouchard, "Least squares magnetic-field optimization for portable nuclear magnetic resonance magnet design," , *IEEE Transactions on*, vol. 44, no. 12, pp. 4582–4590, 2008.

[7] Jeffrey L Paulsen, Louis S Bouchard, Dominic Graziani, and Bernhard Blu, "Volume-selective magnetic resonance imaging using an adjustable , single-sided , portable sensor," *PNAS*, vol. 105, no. 52, pp. 20601–20604, 2008.

[8] B. Blumich, P. Blumer, G. Eidman, A. Guthausen, R. Haken, U. Schmitz, K. Saito, and G. Zimmer, "The NMR-Mouse: Construction, Excitation, and Applications," *1Magnetic resonance imaging*, vol. 16, pp. 479–484, Jan. 1998.

[9] Andrew E Marble, Igor V Mastikhin, Bruce G Colpitts, and Bruce J Balcom, "A constant gradient unilateral magnet for near-surface MRI profiling.," *Journal of magnetic resonance (San Diego, Calif. : 1997)*, vol. 183, no. 2, pp. 228–34, Dec. 2006.

[10] John M Franck, Vasiliki Demas, Rachel W Martin, Louis-S Bouchard, and Alexander Pines, "Shimmed matching pulses: simultaneous control of rf and static gradients for inhomogeneity correction.," *The Journal of chemical physics*, vol. 131, no. 23, pp. 234506, Dec. 2009.

[11] Daniel Topgaard, Rachel W Martin, Dimitris Sakellariou, Carlos A Meriles, and Alexander Pines, ""Shim pulses" for NMR spectroscopy and imaging.," *Proceedings of the National Academy of Sciences of the United States of America*, vol. 101, no. 51, pp. 17576–81, Dec. 2004.

[12] Carlos A Meriles, Dimitris Sakellariou, Henrike Heise, and Alexander Pines, "Approach to High-Resolution ex Situ NMR Spectroscopy," *Science*, vol. 293, no. July, pp. 82–85, 2001.

[13] Carlos a Meriles, Dimitris Sakellariou, Andreas H Trabesinger, Vasiliki Demas, and Alexander Pines, "Zero- to low-field MRI with averaging of concomitant gradient fields.," *Proceedings of the National Academy of Sciences of the United States of America*, vol. 102, no. 6, pp. 1840–2, Feb. 2005.

[14] Nathan Kelso, Seung-Kyun Lee, Louis-S Bouchard, Vasiliki Demas, Michael Mück, Alexander Pines, and John Clarke, "Distortion-free magnetic resonance imaging in the zero-field limit.," *Journal of magnetic resonance (San Diego, Calif. : 1997)*, vol. 200, no. 2, pp. 285–90, Oct. 2009.

[15] Louis-S. Bouchard, "Unidirectional magnetic-field gradients and geometric-phase errors during Fourier encoding using orthogonal ac fields," *Physical Review B*, vol. 74, no. 5, pp. 1–11, Aug. 2006.

[16] Louis-S. Bouchard and M. Anwar, "Synthesis of matched magnetic fields for controlled spin precession," *Physical Review B*, vol. 76, no. 1, pp. 1–10, July 2007.

[17] E Mark Haacke and Robert Brown, "Magnetic Resonance Imaging Physical Principles and Sequence Design," 1999.

[18] Jurgen Reichenbach, Ramesh Venkatesan, Dmitriy Yablonskiy, Michael R Thompson, and E Mark Haacke, "Theory and Application of Static Field Inhomogeneity Effects in Gradient- Echo Imaging," *Journal of Magnetic Resonance Imaging*, vol. 7, pp. 266–279, 1997.

[19] Arnon Neufeld, Yaniv Assaf, Moshe Graif, Talma Hendler, and Gil Navon, "Susceptibility-matched envelope for the correction of EPI artifacts.," *Magnetic resonance imaging*, vol. 23, no. 9, pp. 947–51, Nov. 2005.

[20] Jeffrey A Fessler, "Model-Based Image reconstruction for MRI," *IEEE Signal Processing Magazine*, vol. 936726, no. July, pp. 81–89, 2010.

[21] Bradley P Sutton, Student Member, Douglas C Noll, Jeffrey A Fessler, and Senior Member, "Fast , Iterative Image Reconstruction for MRI in the Presence of Field Inhomogeneities," *IEEE transactions on medical imaging*, vol. 22, no. 2, pp. 178–188, 2003.

[22] Justin Romberg, "Imaging via Compressive Sampling," *IEEE Signal Processing Magazine*, , no. March 2008, pp. 14–20, 2007.

[23] E.J. Candes, J. Romberg, and T. Tao, "Robust uncertainty principles: exact signal reconstruction from highly incomplete frequency information," *IEEE Transactions on Information Theory*, vol. 52, no. 2, pp. 489–509, Feb. 2006.

[24] Dong Liang, Haifeng Wang, and Leslie Ying, "SENSE reconstruction with nonlocal TV regularization.," *Conference proceedings : ... Annual International Conference of the IEEE Engineering in Medicine and Biology Society. IEEE Engineering in Medicine and Biology Society. Conference*, vol. 2009, no. 3, pp. 1032–5, Jan. 2009.

[25] Jian-Feng Cai, Stanley Osher, and Zuowei Shen, "Split Bregman Methods and Frame Based Image Restoration," *Multiscale Modeling & Simulation*, vol. 8, no. 2, pp. 337, 2010.

[26] Tom Goldstein and Stanley Osher, "The Split Bregman Method for L1-Regularized Problems," *SIAM Journal on Imaging Sciences*, vol. 2, no. 2, pp. 323, 2009.

[27] Jeffrey A Fessler, Senior Member, and Bradley P Sutton, "Nonuniform Fast Fourier Transforms Using Min-Max Interpolation," vol. 51, no. 2, pp. 560–574, 2003.